University Library

A gateway to Melbourne's research publications

Minerva Access is the Institutional Repository of The University of Melbourne

Author/s:
Setareh, M;Mousavi Khaleghi, SS;Rodrigo, JA;Crozier, KB

Title:
Generating polymorphic and solenoid beams with an amplitude-type spatial light modulator

Date:
2025

Citation:
Setareh, M., Mousavi Khaleghi, S. S., Rodrigo, J. A. & Crozier, K. B. (2025). Generating polymorphic and solenoid beams with an amplitude-type spatial light modulator. APL Photonics, 10 (12), https://doi.org/10.1063/5.0299055.

Persistent Link:
https://hdl.handle.net/11343/368888

Generating polymorphic and solenoid beams with an amplitude-type spatial light modulator

Maryam Setareh,[1,2] Seyed Saleh Mousavi Khaleghi,[1,2] Jose A. Rodrigo,[4] and Kenneth B. Crozier[1,2,3*]

[1] *Department of Electrical and Electronic Engineering, University of Melbourne, Victoria 3010, Australia*

[2] *Australian Research Council Centre of Excellence for Transformative Meta-Optical System (TMOS), University of Melbourne, VIC 3010, Australia*

[3] *School of Physics, University of Melbourne, Victoria 3010, Australia*

[4] *School of Physics, Complutense University of Madrid, Madrid 28040, Spain*

[*] Corresponding Author: Kenneth.crozier@unimelb.edu.au

Abstract:

Helix-shaped polymorphic beams and solenoid ones are non-diffracting beams generated by the superposition of Bessel beams of specific orders. Their fields rotate around the beam propagation axis and have promising applications in optical forces, where they can be designed to function as either tractor or repulsor beams. Traditionally, phase-only spatial light modulators (SLMs) based on liquid crystal technology have been used for their generation. However, such SLMs have several limitations. They operate within a limited wavelength range, have lower refresh rates (typically 60 Hz, with a maximum of a few hundred Hz), and require linearly polarized light. There is, therefore, a need for an affordable alternative for applications outside the wavelength range of liquid crystal-based SLMs, for those requiring fast refresh rates, or those needing polarization independence. In this work, we show, for the first time to the best of our knowledge, the generation of solenoid and helix-shaped polymorphic beams with an amplitude-type SLM, namely a digital micromirror device (DMD). These address the aforementioned problems faced by liquid crystal-based SLMs. Although there are advantages associated with the use of DMDs, they often suffer from lower efficiency, mainly because many pixels are required to be in the off state. To solve this issue, we apply an intermediate plane holography method. We show that it can be used to generate a complex field helix-shaped polymorphic laser beam with a ~2.5 fold improvement in optical power efficiency.

Key words: DMD, Polymorphic beam, Solenoid beam, Vortex beam, Digital Micromirror Device, Intermediate-plane holography

Introduction

Optical forces, which arise from the interaction between light and matter, are widely used to manipulate microscopic particles. The most established technique based on these forces is optical tweezers, which use a tightly focused laser beam to trap particles. These have enabled a wide range of applications, particularly in biology, such as studies of DNA-protein interactions, manipulating and sorting cells, and investigating the mechanical properties of biological systems[1–5]. The applications of optical forces extend beyond biology. They have also been used in areas such as levitated optomechanics, where particles are trapped in vacuum and used for force sensing and fundamental studies in quantum mechanics[6–9].

In addition to trapping-based approaches, another branch of research explores the use of optical forces to push the particles. This approach opens up possibilities in label-free particle sorting, such as in blood analysis systems that exploit optical pressure differences between cell types[10]. As shown in Ref. [10],

blood components such as lymphocytes, monocytes, granulocytes, and erythrocytes exhibit distinguishable optical pressure responses, enabling their separation without the need for fluorescent labeling. A notable large-scale application for the optical pushing force is the use of laser propulsion to propel lightweight spacecraft for interstellar exploration[11].

The range of applications for optical forces could be expanded even further if light could not only trap or push particles but also pull them toward the light source. Beams capable of this are known as optical tractor beams. Solenoid beams, introduced in 2010, are a type of structured light beam that exhibit a helical intensity pattern and can exert pulling forces on particles along the beam axis[12]. Unlike earlier optical tractor beams, which required particles with specific properties[13,14], with solenoid beams these particles do not need to be specifically-designed for this purpose and can instead be particles commonly used in optical tweezers such as polystyrene or silica particles.

In 2016, Yevick et. al conducted a theoretical study focusing on solenoid beams composed of just two Bessel beams. By analyzing the resulting force field using a photokinetic framework, they derived the conditions necessary for generating pulling forces, demonstrating that a two-component design is sufficient to create a solenoid tractor beam[15].

In 2022, Rodrigo et al. extended this concept by introducing the term 'polymorphic helix-shaped tractor and repulsor beams' [16], referring to beams whose helical structure can deviate from the conventional circular form and exhibit spatially tunable pulling and pushing forces. These structured beams are a particular case of polymorphic beams, which allow independent control over phase and intensity along arbitrary curves[17]. Polymorphic beams have been shown to be effective in particle manipulation at the micro- and nano-scales. Rodrigo et al. demonstrated that solenoid beams, as discussed by Lee et.al[12], are indeed a particular case of polymorphic beams corresponding to circular helices along which intensity is uniform and the phase advances uniformly[16]. This implies that solenoid beams can be regarded as a specific subclass of polymorphic beams.

In both experimental studies, solenoid beams were generated by encoding the appropriate holograms onto phase-only spatial light modulators (SLMs)[12,16]. However, the use of such liquid crystal-based SLMs comes with certain drawbacks. They are typically optimized for a specific wavelength range, often centered around a particular wavelength within the visible to near-infrared spectrum (approximately 400 nm to 1100 nm). The efficiency of an SLM decreases when the laser wavelength deviates significantly from its design wavelength, so when experiments require a different laser wavelength, the SLM may not provide optimal performance. Additionally, such SLMs have relatively low refresh rates (typically around 60 Hz), which limits their ability to generate dynamic light fields. They also require linearly polarized light, making them less versatile for applications that demand polarization-independent control. Therefore, there is a need for a more affordable alternative that offers broader wavelength compatibility, higher refresh rates, and polarization independence.

Here, we generate solenoid beams using amplitude-type spatial light modulators, namely digital micromirror devices (DMDs). In addition to being cost-effective, DMDs offer several advantages Unlike SLMs, which operate within a limited wavelength range, DMDs function effectively across a wide range of wavelengths. Furthermore, while most SLMs require linear polarization, DMDs are polarization insensitive[18–20]. Their high refresh rate also makes them a suitable alternative for applications that require dynamic beam shaping.

This article is structured as follows. We begin with an introduction to helix-shaped polymorphic beams, including the sub-class of solenoid beams. Then, we describe how DMDs are used to generate the beams. We present both simulation and experimental results, focusing on generating solenoid beams with different numbers of spirals, namely one, two, and three. Theoretical beam profiles are computed using the Fresnel propagation method. The experimental results show good agreement with the theoretical intensity beam profiles, demonstrating that even cost-effective DMDs can successfully

generate these beams. Beam propagation is also mapped over distance to better illustrate the helical nature of our beams. We then address the efficiency limitation of amplitude-only modulators like DMDs, where much of the light is lost because many micromirrors must be turned off when encoding complex field patterns. To do so, we generate a complex-field polymorphic beam and apply intermediate-plane holography by encoding the back-propagated polymorphic beam onto the DMD. This can improve the efficiency of the generated beam if an appropriate distance is chosen for the back propagation. The paper concludes with a discussion on potential areas for future research.

Overview and Results

Solenoid Beams

Solenoid beams are non-diffracting structured beams with intensity peaks that rotate around the optical axis. These beams can be generated by the superposition of Bessel beams with different orders. Their distinctive ability to exert tailored optical forces has made them an intriguing topic in the field of particle manipulation[12,15,16].

In Yevick et al.'s work, two-component solenoid beams were introduced, showing that the superposition of just two Bessel beams is sufficient to generate a solenoid beam[15]. Yevick et al. noted that to optimize the interference of these two Bessel beams, each carrying different orbital angular momentum m and n and convergence angles of α and β, they should contribute equally to the amplitude "u_0"[15]. Therefore, the amplitude and phase of the solenoid beam at r=R can be expressed as[15]:

$$u(r)|_{r=R} = u_0 \cos\left(\frac{m-n}{2}\left[\theta - kz\frac{\cos\alpha - \cos\beta}{m-n}\right]\right) \quad (1)$$

$$\phi(r)|_{r=R} = \frac{m+n}{2}\theta + \frac{\cos\alpha + \cos\beta}{2}kz \quad (2)$$

where R is the radial distance from the beam axis at which constructive interference of the modes occurs, resulting in an intensity maximum that forms a stable trapping region. Here, k is the wavenumber, and z is the propagation direction[15].

Helix-shaped Polymorphic Beams

Helix-shaped polymorphic beams can be regarded as a generalized form of solenoid beams. They are non-diffracting and exhibit intensity maxima that rotate around the beam axis. They can be engineered to function as either repulsor or tractor beams. These beams are generated from Bessel beams and offer the ability to modify the geometry of the transverse intensity profile[16]. This is achieved by incorporating the superformula, a mathematical expression that allows the description of complex shapes using a single equation, into the field definition. Beams with intricate geometries, such as triangular or star-like patterns [16,17,21], can be generated.

Despite being based on Bessel beams, helix-shaped polymorphic beams can only be formed using Bessel beams of specific orders. The allowed order depends on desired beam parameters such as the winding number l, helix pitch γ, and the wavelength of light. The following condition must be satisfied for the generation of a polymorphic beam with a positive helix pitch (γ>0; counterclockwise rotation)[16]:

$$\gamma > 0; l - k\gamma < n < l \quad (3)$$

Here, l is the winding number, corresponding to a phase accumulation of $2\pi l$ over one complete helical loop, and k is the wavevector. The helix pitch γ corresponds to the height $2\pi\gamma$ of one helical loop. It should also be noted there is a limit for other parameters as well. For instance, to make sure that the generated helix-shaped polymorphic beam acts as a tractor beam, the condition for a winding number $|l| < kR$ should also be satisfied where R is the radius of the helix[16].

Digital Micromirror Devices

DMDs, primarily used in projection systems[22], have found widespread use in a variety of advanced applications[23,24]. These include single-pixel imaging[25,26], which is particularly beneficial for biomedical[27,28] and spectral imaging[29], maskless lithography[30,31], and wavefront shaping[32–34].

As discussed, DMDs offer several advantages over SLMs, including lower cost, broader wavelength compatibility, and faster refresh rates, making them suitable for a wider range of applications.

A DMD consists of an array of micromirrors that can tilt diagonally to either +12° (on state) or -12° (off state). Due to this two-state operation system, they function as binary amplitude-type modulators. When in the on state, the micromirror array reflects light to one side, while mirrors in the off state direct the beam to the opposite side relative to the incident beam [20].

Although DMDs are inherently amplitude modulators, several research groups have developed techniques that enable the encoding of both amplitude and phase information onto the DMD. One well-known method for achieving this is the Binary Lee method[20,35].

In this method, to generate a beam with an amplitude A and a phase φ, the following binary mask hologram is used[20,35]:

$$H_{DMD}(x,y) = \frac{1}{2} + \frac{1}{2}\,\mathrm{sign}\left\{\cos\left[2\pi\left(\frac{x}{\lambda_x} + \frac{y}{\lambda_y}\right) + \varphi(x,y)\right] - \cos\left(arcsin\left[A(x,y)\right]\right)\right\} \qquad (4)$$

In this equation H_{DMD} represents the DMD hologram mask, sign refers to the sign function, and λ_x and λ_y are the carrier wave's period along the x and y directions, respectively, and should not be confused with the laser wavelength.

Simulation and experimental results

Phase-only solenoid beams

To encode the desired beam holograms onto the DMD, we use the Binary Lee method as described in the previous section. This encoding technique enables the modulation of both amplitude and phase. In this section, we consider solenoid beams. These require only phase modulation. We therefore assume $\left[A(x,y)\right] = 1$ across the entire beam, effectively removing the amplitude term from the equation. However, this does not limit the generality of the approach and later on we will encode both amplitude and phase onto our DMD to generate a polymorphic beam. As mentioned earlier, this method requires a carrier phase, which must be chosen carefully to separate the diffraction orders. The carrier period should not be too short, as this can lead to the generation of ghost images[20]. To begin, we generate a one-spiral solenoid beam, with the binary hologram pattern encoded onto our DMD, as shown in Fig. 1(a). This mask is generated with a carrier period of 50 micrometers. We use the experimental setup schematically illustrated in Fig. 1b to produce our solenoid beam. The beam from an infrared laser (wavelength: 1064 nm, Laser Ventus Quantum) illuminates the DMD (DLP2000, Texas Instruments). The first diffraction order generated by the DMD is captured by a complementary metal oxide semiconductor (CMOS) camera. The camera is mounted on a translation stage, and images are captured with a step size of approximately 2 mm.

Theoretical calculations are performed using MATLAB, where we use a Fresnel propagation function to generate intensity plots at various axial distances. Initially, we do calculations for a one-spiral beam generated by two Bessel beams, with orders of -5 and -4 and convergence angles of 5 mrad and 4 mrad, respectively. Fig.2 (a-d) show the in-plane intensity profiles at different distances (6 cm, 9 cm, 12 cm and 19.5 cm) from the hologram. To clearly observe the helical nature of the solenoid beam, we map the beam from approximately 4.5 cm to 22 cm and generate isosurface plots, as shown in Fig. 2 (e). Fig.

2 (f-i) shows the experimental results. From the captured images, we produce the isosurface plot shown in Fig. 2(j).

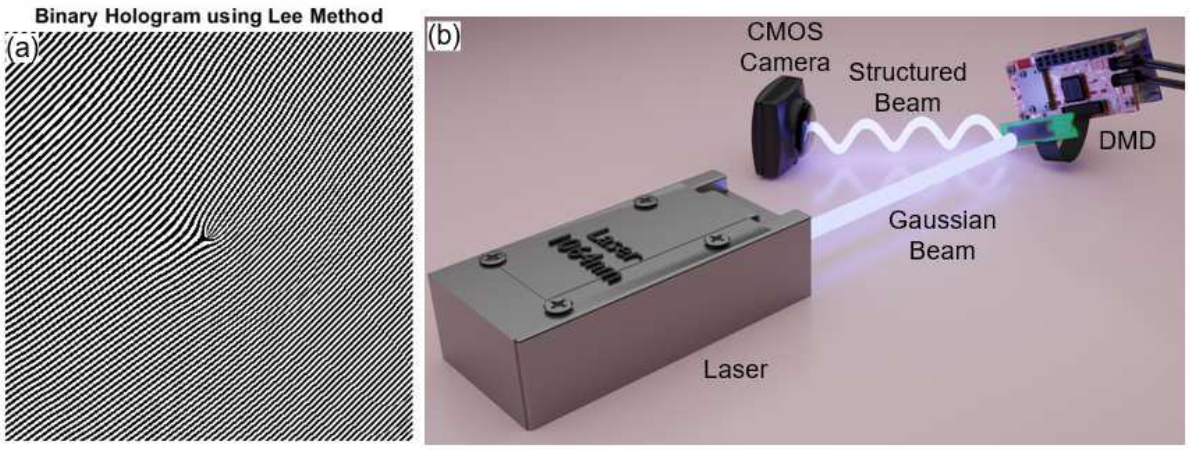

Figure 1(a) Hologram encoded onto the DMD to generate one-spiral solenoid beam. (b) Schematic of the experimental setup

It is important to note that DMDs, like many other optical components, can introduce aberrations into the optical system. One of the primary aberrations induced by a DMD is astigmatism. Therefore, to improve the agreement between experimental results and simulations, aberration correction is required. In this work, we employ Zernike polynomials, which are suitable for representing the shape of aberrated wavefronts. All experimental results presented here are obtained after applying polynomial-based correction. The encoded phase is given by the equation:

$$\varphi_{encoded} = \varphi_{original} + \varphi_{correction} \tag{5}$$

Where $\varphi_{original}$ is the phase of the desired beam, and $\varphi_{correction}$ is the correction term derived from the Zernike astigmatism modes[36]. Specifically, $\varphi_{correction} = \sum_j C_j z_j$, where z_j is the Zernike

polynomial and C_j is the corresponding weighting coefficient, chosen to optimize the similarity between experimental images and simulations[20]. This approach is similar to the method described in Ref. [20]. As an example, after applying the Zernike polynomials in Fig. 2 (a), the experimental aspect ratio (measured along two orthogonal directions through the beam center) matches the simulation within about 4% error.

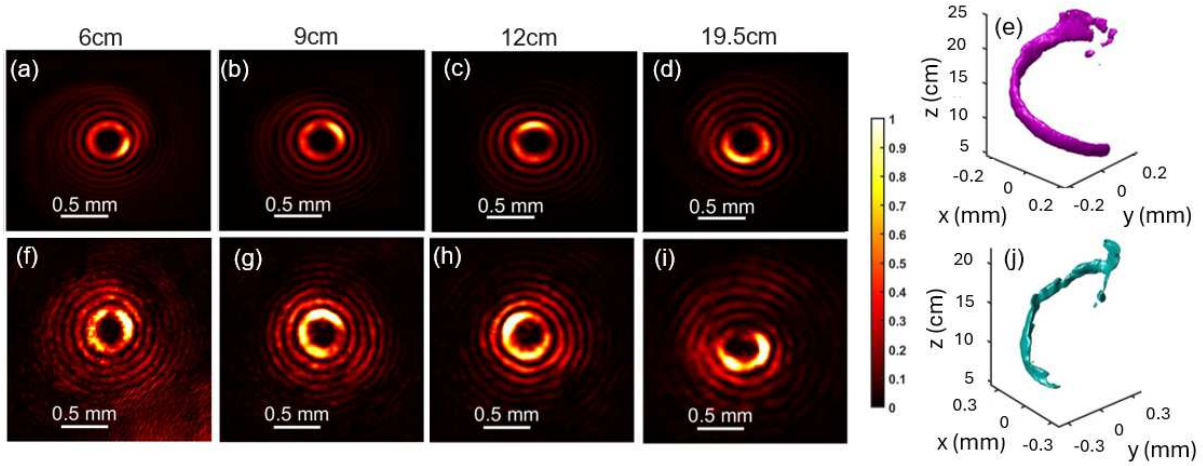

Figure 2: One-spiral solenoid beam. Top row (a-d): Simulated intensity profiles captured at distances of 5.5, 9, 12 and 19.5 cm, respectively. (e) Simulated isosurface plot. Bottom row (f-i): Corresponding experimental results and (j) experimental isosurface obtained at 96% of peak intensity.

To demonstrate that the ability to generate solenoid beams using our DLP 2000 is not limited to a single beam configuration, we perform experiments with other solenoid beams, such as a two-spiral beam, as shown in Fig. 3. This beam is generated by Bessel beams with orders (winding numbers) of -5 and -3 and convergence angles of 5 mrad and 4 mrad, respectively. As with the previous results, there is good agreement between the experimental and simulation data. Both sets of data demonstrated similar behavior, with the spirals exhibiting comparable rotational distances, as well as matching beam sizes. However, the experimental data displays some jaggedness in the spirals, which could be attributed to slight mis-alignment of the beam between camera frames during image capture, possibly meaning that the images are not exactly centered (i.e. the desired beam generated by the DMD appears in a diffraction order at an angle, and the camera may not be perfectly aligned to this angle).

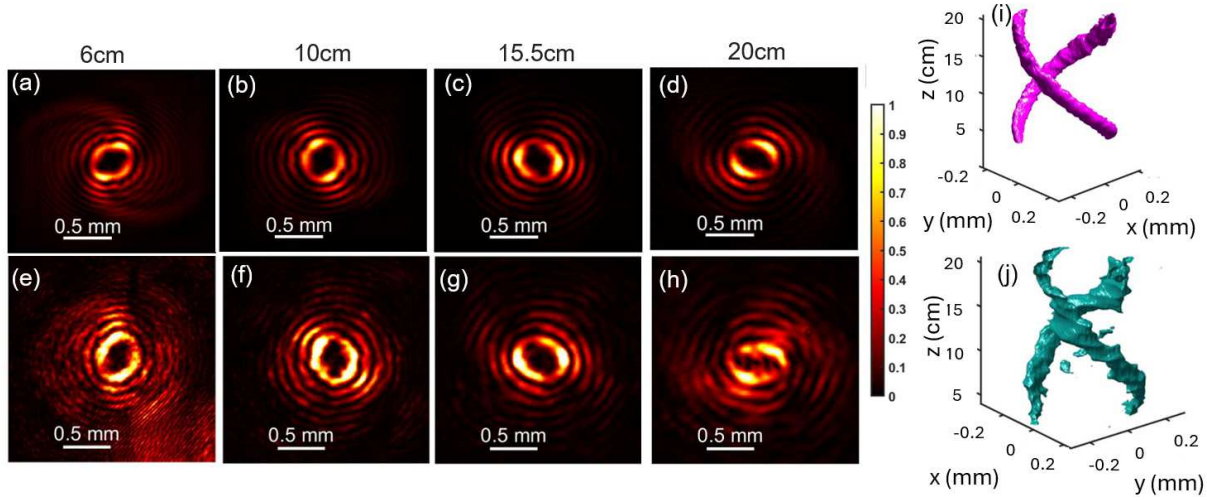

Figure 3: Two-spiral solenoid beam. Top row (a-d): Simulated intensity profiles captured at distances of 6, 10, 15.5 and 20 cm respectively. Bottom row (e-h): Corresponding experimental results. (i)Simulated isosurface plot. (j) Experimental isosurface obtained at 80% of peak intensity.

In a previous study, we generated a solenoid beam using a metasurface[37]. For comparison, we repeat the experiment with a similar solenoid beam, using orders of -10 and -7 and convergence angles of 5 mrad and 4 mrad, respectively, and observe the generation of a triple-helix solenoid beam as shown in Fig. 4 (a-h). In Fig. 4 (i–p), we demonstrate a spiral solenoid beam generated using Bessel beams of different orders compared to those used in Fig. 2. Specifically, this beam is formed by superposition of

Bessel beams of orders -4 and -3, with convergence angles of 5 mrad and 0.0075 rad, respectively. As the difference between orders of Bessel beams takes a value of unity, a single spiral beam is expected, and this is confirmed experimentally. The recorded intensity patterns clearly show the rotation of the intensity maxima along the propagation direction.

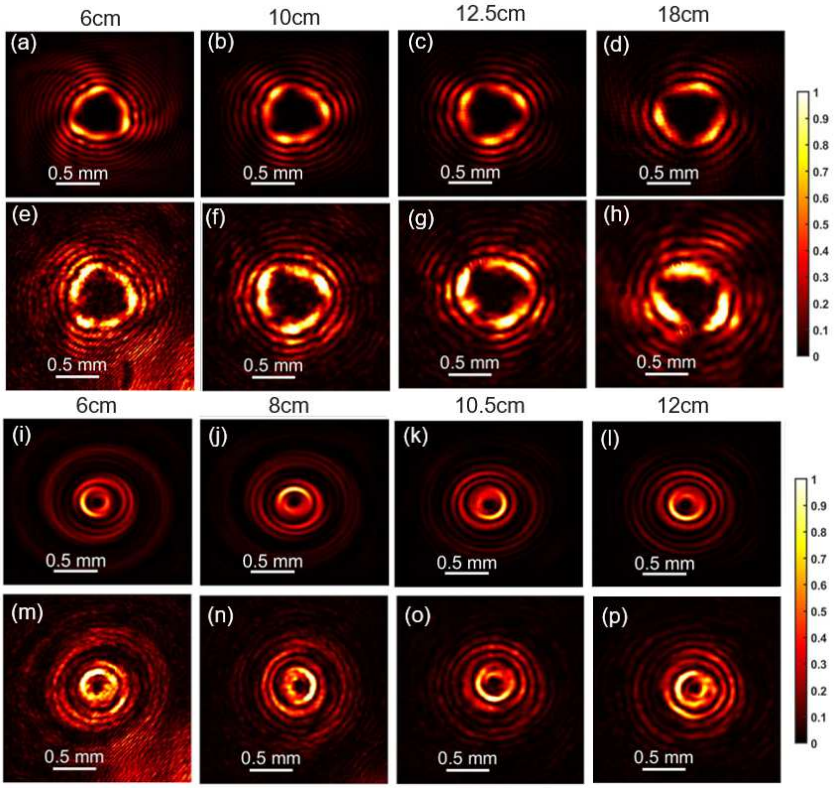

Figure 4: Triple helix solenoid beam (a-h). Top row (a-d): Simulated intensity profiles captured at distances of 6, 10, 12.5 and 18 cm respectively. Bottom row (e-h): Corresponding experimental results. One spiral solenoid beam (i-p). Top row (i-l): Simulated intensity profiles captured at distances of 6, 8, 10.5 and 12 cm respectively. Bottom row (m-p): Corresponding experimental result.

Complex-field polymorphic beam

In the previous section, we generated a phase-only solenoid beam by encoding its phase profile onto the DMD. In this section, we aim to generate a polymorphic beam with a complex field. To achieve this, we first perform simulations to generate a helix-shaped polymorphic beam with a winding number of -7.6. As described in Ref. [16], a physically realizable helix-shaped polymorphic beam can be represented by the equation shown below, from which the phase and amplitude of the desired beam can be extracted[16]:

$$E(r_0,\varphi) \propto \frac{z_{eff}}{|\gamma|}\sum_{n=-\infty}^{n=\infty} \mathrm{i}^n \exp(\mathrm{i}n\varphi) J_n\left(\frac{kr_0}{\sqrt{f^2+r_0^2}}R\right)\mathrm{sinc}\left[\left(l-n-\gamma\frac{kf}{\sqrt{f^2+r_0^2}}\right)\frac{z_{eff}}{2|\gamma|}\right] \qquad (6)$$

In the above equation, f denotes the focal length of the lens, z_{eff} is the effective length of the helix beam and J_n denotes the Bessel beam of order n[16]. Using the same encoding technique as previously described, the complex field; comprising both amplitude and phase; is converted into an amplitude-only hologram suitable for encoding onto the DMD. Figures 5a and 5b show the amplitude and phase of the electric field required to generate a helix-shaped polymorphic beam with a winding number of -7.6. In Fig. 5c, we present the simulated beam obtained using the amplitude and phase distributions shown in

Figs. 5a and 5b. Figure 5d displays the experimental intensity pattern captured at the Fourier plane of a lens with a focal length of 25 cm, following the encoding of the amplitude (Fig. 5a) and phase (Fig. 5b) onto the DMD.

As is evident from Fig. 5a, the non-zero regions of the amplitude pattern are relatively narrow and occupy a small fraction of the area, leading to low power efficiency, as a significant portion of the DMD pixels are in the off state. To address this limitation, we apply a back-propagation technique, in which the desired beam is numerically propagated backward using Fresnel propagation (Fig. 5e), and the resulting field is encoded onto the DMD. This approach effectively enhances the overall power efficiency and is conceptually similar to the approach described in Ref. [38], where a comparable technique was implemented using phase-only SLMs. That study also mentions that employing intermediate-plane holograms can enhance diffraction efficiency as well as the purity of propagation-invariant modes, which in turn helps to extend their effective non-diffracting distance[38].

As shown in Fig. 5f, the number of active (ON) pixels increases as the beam is propagated either backward or forward, reaching a maximum at approximately 400 mm. In our implementation, we backpropagate the beam by 200 mm and physically shift the DMD to this plane. The corresponding experimental result is shown in Fig. 5g. A comparison between Fig. 5g (back-propagated case) and Fig. 5d (original case), under the same incident power and the same camera settings, clearly demonstrates the effectiveness of the proposed approach, with the measured power increasing from 0.29 mW to 0.62 mW.

The intermediate plane method can improve the output intensity in both phase-type SLM and DMD systems—not just DMDs. In the case of polymorphic beam generation, both phase-type SLM and DMD approaches typically require relatively high laser power, since the Bessel beam on the SLM uses only a small number of pixels. Applying this intermediate plane technique can help reduce the laser power requirement by enhancing the utilization of available pixels.

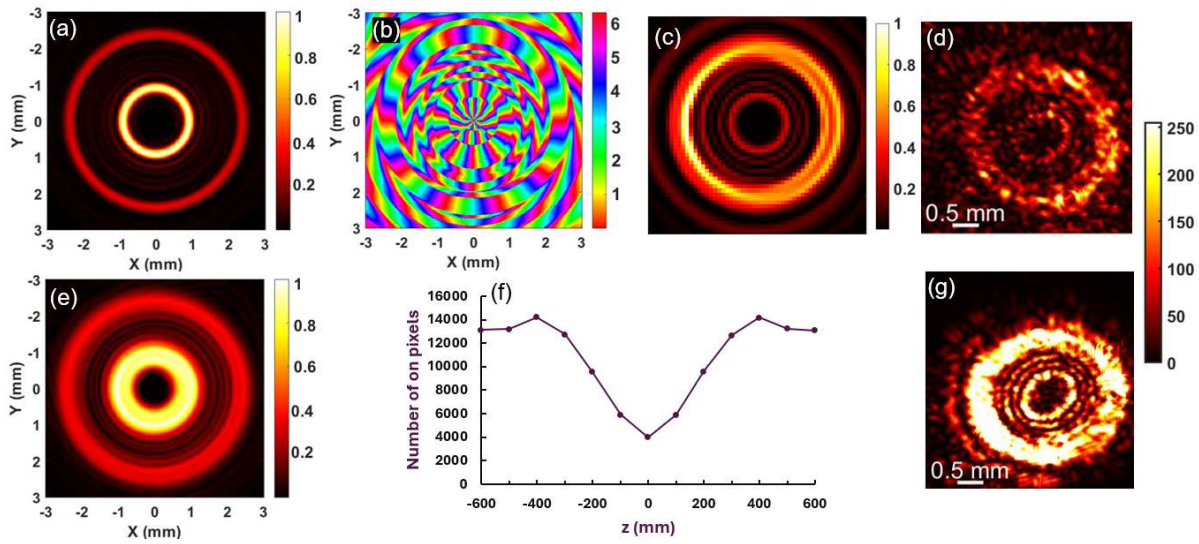

Figure 5: (a) Amplitude of the electric field at z=0. (b) Phase of the electric field at z=0. (c) Simulated beam profile at the Fourier plane, generated using the amplitude in (a) and phase in (b). (d) Experimental intensity distribution at the Fourier plane of the lens, generated using the DMD. (e) Amplitude of the back-propagated beam at z=−200 mm. (f) Number of active (ON) pixels on the DMD as a function of propagation distance. (g) Experimental intensity distribution at the Fourier plane of the lens using the hologram encoded from the back-propagated field.

Discussions

In conclusion, we demonstrated the possibility of generating solenoid beams using an amplitude-type spatial light modulator (DLP 2000). We were able to map the beam propagation over centimeter-scale distances for various solenoid beams. We used the Binary Lee method for encoding; however,

alternative approaches exist. One such approach is the superpixel method, where groups of pixels form a block called a superpixel, and different on/off combinations within each superpixel encode a specific complex field value. As reported in Ref. [39], both the Binary Lee and superpixel methods provide similar efficiency, and for low-resolution targets, both can generate fields with similarly high fidelities. For high-resolution target fields, the superpixel method can achieve higher fidelity, although this comes at the cost of reduced spatial resolution[39]. Using the 360 × 360-pixel DMD in our setup, we considered the Binary Lee method to be the better option. Additionally, the superpixel method requires a lookup table, which adds experimental complexity. Therefore, for applications requiring dynamic hologram generation, the Binary Lee method may be preferred, as it does not require handling a lookup table.

We demonstrated a technique to enhance the optical power efficiency of helix-shaped polymorphic beams generated by the DMD. Experimental results show that backpropagating the beam to -200 mm improves the power efficiency by more than a factor of two. The concept of using a back-propagated beam can be applied to beams whose intensity changes during free-space propagation. The optimal propagation distance depends on the beam structure and can be found numerically by propagating the target field, generating holograms for each plane, and identifying the plane that maximizes the number of DMD pixels in the on-state. As shown in Fig. 5(f), this dependence is approximately symmetric for forward and backward propagation, allowing either approach depending on the experimental geometry.

Despite the relatively low efficiency of DMDs, which also depends on the number of mirrors in the "on" state, they offer several advantages over liquid crystal-based SLMs, including polarization insensitivity, a higher refresh rate, and lower cost, making them a suitable choice for a broader range of experiments. The polarization insensitivity of DMDs simplifies their integration into complex or uncontrolled optical environments, such as fiber-based systems where maintaining polarization is difficult. Additionally, the broad spectral range of DMDs enables their use in multi-wavelength and hyperspectral imaging systems. Their fast refresh rates also make them well-suited for applications like single-pixel cameras.

However, despite these advantages, the beam quality achievable with phase-type SLMs still surpasses that of DMDs. While phase type SLMs can deliver both high beam quality and support relatively high femtosecond laser powers[40], DMDs may still present a distinct advantage when even higher power thresholds are required, especially in applications involving ultra-intense pulsed lasers. In such regimes, where phase-type SLMs devices become unsuitable due to power limitations, DMDs could enable the extension of solenoid tractor beam applications to ultra-intense laser conditions. However, this comes at the cost of beam quality due to the binary nature of DMD holograms, which limits simultaneous amplitude and phase encoding. Beam quality could be improved by using DMDs with a higher number of pixels, which would also allow the implementation of superpixel-based encoding methods with better spatial resolution and improved fidelity, as discussed earlier. One of the most notable applications of solenoid beams is the generation of tractor and repulsor beams, which may be challenging to observe using a DLP 2000 due to the high-power requirement and the beam quality issue as discussed. However, additional applications may emerge. For instance, as discussed in Ref. [16], these helix-shaped beams might be used in photopolymerization-based fabrication of sophisticated structures[16].

Acknowledgements. This work was supported by the Australian Research Council Centre of Excellence for Transformative Meta-Optical Systems (Project No. CE200100010).

Disclosures. The authors declare no competing financial interests.

Author Contributions.
Kenneth B. Crozier: Conceptualization (overall project idea), Supervision, Writing – Review & Editing.
Maryam Setareh: Investigation (conducted the experiments), Writing – Original Draft.

Jose A. Rodrigo: Conceptualization (idea of back propagation), Writing – Review & Editing.
Seyed Saleh Mousavi Khaleghi: Investigation (assisted in the experiments).

Data Availability. Data may be obtained from the authors upon reasonable request.

References

(1) Ashkin, Arthur, and James M. Dziedzic. "Optical Trapping and Manipulation of Viruses and Bacteria." Science, 235 (4795), 1517-1520(1987).

(2) Johansen, P. L.; Fenaroli, F.; Evensen, L.; Griffiths, G.; Koster, G. Optical Micromanipulation of Nanoparticles and Cells inside Living Zebrafish. Nat Commun, 7(1),10974 (2016). https://doi.org/10.1038/ncomms10974.

(3) Bustamante, C. J.; Chemla, Y. R.; Liu, S.; Wang, M. D. Optical Tweezers in Single-Molecule Biophysics. Nature Reviews Methods Primers, 1(1), 2021. https://doi.org/10.1038/s43586-021-00021-6.

(4) Zheng, B.; Li, C. Y.; Huang, S.; Zhang, Z. L.; Wu, Q. S.; Pang, D. W.; Tang, H. W. Optical Tweezers Assisted Analyzing and Sorting of Tumor Cells Tagged with Fluorescence Nanospheres in a Microfluidic Chip. Sens Actuators B Chem, 368,132173 (2022). https://doi.org/10.1016/j.snb.2022.132173.

(5) Yadav, D. S.; Savopol, T. Optical Tweezers in Biomedical Research – Progress and Techniques. J Med Life, 17 (11), 978–993 (2024). https://doi.org/10.25122/jml-2024-0316.

(6) Ranjit, G.; Cunningham, M.; Casey, K.; Geraci, A. A. Zeptonewton Force Sensing with Nanospheres in an Optical Lattice. Phys Rev A (Coll Park), 93 (5),053801(2016). https://doi.org/10.1103/PhysRevA.93.053801.

(7) Monteiro, F.; Li, W.; Afek, G.; Li, C. L.; Mossman, M.; Moore, D. C. Force and Acceleration Sensing with Optically Levitated Nanogram Masses at Microkelvin Temperatures. Phys Rev A (Coll Park), 101 (5), 053835 (2020). https://doi.org/10.1103/PhysRevA.101.053835.

(8) Vijayan, J.; Piotrowski, J.; Gonzalez-Ballestero, C.; Weber, K.; Romero-Isart, O.; Novotny, L. Cavity-Mediated Long-Range Interactions in Levitated Optomechanics. Nat Phys, 20 (5), 859–864 (2024). https://doi.org/10.1038/s41567-024-02405-3.

(9) Hempston, D.; Vovrosh, J.; Toroš, M.; Winstone, G.; Rashid, M.; Ulbricht, H. Force Sensing with an Optically Levitated Charged Nanoparticle. Appl Phys Lett 2017, 111 (13). https://doi.org/10.1063/1.4993555.

(10) Hebert, C. G.; Terray, A.; Hart, S. J. Toward Label-Free Optical Fractionation of Blood-Optical Force Measurements of Blood Cells. Anal Chem, 83 (14), 5666–5672 (2011). https://doi.org/10.1021/ac200834u.

(11) Michaeli, L.; Gao, R.; Kelzenberg, M. D.; Hail, C. U.; Merkt, A.; Sader, J. E.; Atwater, H. A. Direct Radiation Pressure Measurements for Lightsail Membranes. Nat Photonics, 19 (4), 369–377 (2025). https://doi.org/10.1038/s41566-024-01605-w.

(12) Lee, S.-H.; Roichman, Y.; Grier, D. G. Optical Solenoid Beams. Optics Express, 18(7), Pp.6988-6993 (2010).

(13) Shvedov, V.; Davoyan, A. R.; Hnatovsky, C.; Engheta, N.; Krolikowski, W. A Long-Range Polarization-Controlled Optical Tractor Beam. Nat Photonics, 8 (11), 846–850 (2014). https://doi.org/10.1038/NPHOTON.2014.242.

(14) Kajorndejnukul, V.; Ding, W.; Sukhov, S.; Qiu, C. W.; Dogariu, A. Linear Momentum Increase and Negative Optical Forces at Dielectric Interface. Nat Photonics, 7 (10), 787–790 (2013). https://doi.org/10.1038/nphoton.2013.192.

(15) Yevick, A.; Ruffner, D. B.; Grier, D. G. Tractor Beams in the Rayleigh Limit. Phys Rev A (Coll Park), 93 (4), 043807(2016). https://doi.org/10.1103/PhysRevA.93.043807.

(16) Rodrigo, J. A.; Martínez-Matos, Ó.; Alieva, T. Helix-Shaped Tractor and Repulsor Beams Enabling Bidirectional Optical Transport of Particles En Masse. Photonics Res, 10 (11), 2560 (2022). https://doi.org/10.1364/prj.468060.

(17) Rodrigo, J. A.; Alieva, T. Polymorphic Beams and Nature Inspired Circuits for Optical Current. Sci Rep, 6(1),35341(2016). https://doi.org/10.1038/srep35341.

(18) Rosales-Guzmán, C.; Hu, X. B.; Selyem, A.; Moreno-Acosta, P.; Franke-Arnold, S.; Ramos-Garcia, R.; Forbes, A. Polarisation-Insensitive Generation of Complex Vector Modes from a Digital Micromirror Device. Sci Rep, 10 (1),10434 (2020). https://doi.org/10.1038/s41598-020-66799-9.

(19) Li, R.; Zhu, X.; Tu, Y.; Lin, Z.; Liu, Z.; Liu, T.; Ren, Y. Generation of High Radial Node Vector Vortex Beams Based on Digital Micromirror Device. Opt Laser Technol, 171,110457 (2024). https://doi.org/10.1016/j.optlastec.2023.110457.

(20) Perumal, L.; Forbes, A. Broadband Structured Light Using Digital Micro-Mirror Devices (DMDs): A Tutorial. Journal of Optics (United Kingdom), 25 (7), 074003 (2023). https://doi.org/10.1088/2040-8986/acd563.

(21) Rodrigo, J. A.; Alieva, T. Vector Polymorphic Beam. Sci Rep, 8 (1), 7698 (2018). https://doi.org/10.1038/s41598-018-26126-9.

(22) Dudley, D.; Duncan, W.; Slaughter, J. Emerging Digital Micromirror Device (DMD) Applications DLP TM Products New Applications; 2003. http://spiedl.org/terms.

(23) Wang, Z.; Yang, W.; Qin, Y.; Liang, W.; Yu, H.; Liu, L. Digital Micro-Mirror Device - Based Light Curing Technology and Its Biological Applications. Optics and Laser Technology., 143, 107344 (2021). https://doi.org/10.1016/j.optlastec.2021.107344.

(24) Yoon, T.; Kim, C. S.; Kim, K.; Choi, J. ryul. Emerging Applications of Digital Micromirror Devices in Biophotonic Fields. Optics and Laser Technology. 104, 17–25 (2018). https://doi.org/10.1016/j.optlastec.2018.02.005.

(25) Sun, M. J.; Edgar, M. P.; Gibson, G. M.; Sun, B.; Radwell, N.; Lamb, R.; Padgett, M. J. Single-Pixel Three-Dimensional Imaging with Time-Based Depth Resolution. Nat Commun, 7(1), 12010 (2016). https://doi.org/10.1038/ncomms12010.

(26) Mousavi Khaleghi, S. S.; Balendhran, S.; Azar, N. S.; Sulejman, S.; Roberts, A.; Crozier, K. B. High Resolution, Low Noise and Full Color Single Pixel Imaging Camera Using Cyclic Patterns. In 2023 Conference on Lasers and Electro-Optics (CLEO); 2023; pp 1–2.

(27) Huynh, N.; Lucka, F.; Zhang, E.; Betcke, M.; Arridge, S. R.; Beard, P. C.; Cox, B. T. Single-Pixel Camera Photoacoustic Tomography. J Biomed Opt, 24 (12), 1(2019). https://doi.org/10.1117/1.jbo.24.12.121907.

(28) Dutta, R.; Manzanera, S.; Gambín-Regadera, A.; Irles, E.; Tajahuerce, E.; Lancis, J.; Artal, P. Single-Pixel Imaging of the Retina through Scattering Media. Biomed Opt Express,10 (8), 4159 (2019). https://doi.org/10.1364/boe.10.004159.

(29) Tao, C.; Zhu, H.; Wang, X.; Zheng, S.; Xie, Q.; Wang, C.; Wu, R.; Zheng, Z. Compressive Single-Pixel Hyperspectral Imaging Using RGB Sensors. Opt Express, 29 (7), 11207 (2021). https://doi.org/10.1364/oe.416388.

(30) Dinh, D. H.; Chien, H. L.; Lee, Y. C. Maskless Lithography Based on Digital Micromirror Device (DMD) and Double Sided Microlens and Spatial Filter Array. Opt Laser Technol, 113, 407–415 (2019). https://doi.org/10.1016/j.optlastec.2019.01.001.

(31) Lee, W. F.; Wu, C. Y.; Lee, Y. C. High Performance DMD Lithography Based on Oblique Scanning, Pulse Lighting, and Optical Distortion Calibration. Opt Laser Technol **2025**, 183,112388 (2025). https://doi.org/10.1016/j.optlastec.2024.112388.

(32) Ayoub, A. B.; Psaltis, D. High Speed, Complex Wavefront Shaping Using the Digital Micro-Mirror Device. Sci Rep, 11(1), 18837 (2021).https://doi.org/10.1038/s41598-021-98430-w.

(33) Georgieva, A.; Belashov, A. V.; Petrov, N. V. Optimization of DMD-Based Independent Amplitude and Phase Modulation by Analysis of Target Complex Wavefront. Sci Rep, 12(1), 7754 (2022). https://doi.org/10.1038/s41598-022-11443-x.

(34) Mitchell, K. J.; Turtaev, S.; Padgett, M. J.; Čižmár, T.; Phillips, D. B. High-Speed Spatial Control of the Intensity, Phase and Polarisation of Vector Beams Using a Digital Micro-Mirror Device. Opt Express, 24 (25), 29269 (2016). https://doi.org/10.1364/oe.24.029269.

(35) Chen, Y.; Fang, Z.-X.; Ren, Y.-X.; Gong, L.; Lu, R.-D. Generation and Characterization of a Perfect Vortex Beam with a Large Topological Charge through a Digital Micromirror Device. Appl Opt, 54 (27), 8030 (2015). https://doi.org/10.1364/ao.54.008030.

(36) Mahajan, V. N. Zernike Polynomial and Wavefront Fitting. In Optical Shop Testing; John Wiley & Sons, Ltd, 2007; pp 498–546. https://doi.org/https://doi.org/10.1002/9780470135976.ch13.

(37) Setareh, M.; De Gille, R.; Cadusch, J.; Wen, D.; Kim, S.; Crozier, K. B. High Efficiency Triple-Helix Solenoid Beam Generated by Dielectric Metasurface. ACS

Photonics, 11(9), 3486-3491(2024).
https://doi.org/10.1021/acsphotonics.4c00874

(38) Mondal, A.; Yevick, A.; Blackburn, L. C.; Kanellakopoulos, N.; Grier, D. G. Projecting Non-Diffracting Waves with Intermediate-Plane Holography. Opt Express, 26 (4), 3926 (2018). https://doi.org/10.1364/oe.26.003926.

(39) Goorden, S. A.; Bertolotti, J.; Mosk, A. P. Superpixel-Based Spatial Amplitude and Phase Modulation Using a Digital Micromirror Device. *Opt Express*, *22* (15), 17999 (2014). https://doi.org/10.1364/oe.22.017999.

(40) Franco, E.; Martínez-Matos, Ó.; Rodrigo, J. A. Curve-Shaped Ultrashort Laser Pulses with Programmable Spatiotemporal Behavior. Optica, 10 (3), 379 (2023). https://doi.org/10.1364/optica.478086.